



A magnetically recyclable heterogeneous BINOL organocatalyst for the asymmetric aldol reaction



Yean Kee Lee^{a,*}, Kheng Soo Tay^b, Vannajan Sanghiran Lee^a, Noorsaadah Abd. Rahman^a

^a Drug Design and Development Research Group, Department of Chemistry, Faculty of Science, University of Malaya, 50603 Kuala Lumpur, Malaysia

^b Environmental Research Group, Department of Chemistry, Faculty of Science, University of Malaya, 50603 Kuala Lumpur, Malaysia

ARTICLE INFO

Article history:

Received 25 March 2015

Received in revised form 3 June 2015

Accepted 4 June 2015

Available online 7 June 2015

Keywords:

Magnetic iron oxide particles

Catalyst

Reusability

BINOL

Immobilisation

ABSTRACT

A chiral organocatalyst derived from (R)-1,1'-bi-2-naphthol (BINOL) was developed for immobilisation onto magnetic iron oxide particle (MIOP). This heterogeneous organocatalyst was characterised using infrared spectroscopy (FTIR), thermal gravimetric analysis (TGA) and scanning electron microscope (SEM). The performance of BINOL-grafted MIOP (BINOL-MIOP) was then evaluated using aldol reaction between benzaldehydes and cyclic ketones. Comparative studies between homogeneous versus heterogeneous aldol reaction revealed the similar reactivity for both reaction systems. The reaction system mediated by BINOL-MIOP was versatile to produce aldol adducts in moderate-to-good yields (45–99%) from different benzaldehydes and cyclic ketones. In addition, more *syn* adducts were produced in most cases. Up to 35% ee was observed in *anti* adducts, despite that a higher 50% ee of *anti* adduct was observed in the homogeneous reaction system. This observation was supported by the results obtained from the molecular modelling, which revealed the reduced selectivity in the heterogeneous system that was possibly caused by the torsional angle distortion of BINOL after immobilisation. In contrast to the free-BINOL, the distorted-BINOL exhibited lower tendency to form a complex with aldehyde, thereby reducing the selectivity that the free-BINOL could deliver. In addition, the reaction system mediated by BINOL-MIOP was exhibiting an excellent reusability for up to 10 cycles of reactions.

© 2015 Elsevier B.V. All rights reserved.

1. Introduction

Organocatalysis has emerged as one of the powerful tools for organic reactions [1]. Due to the toxic nature of heavy metal-based catalysts, the development of organocatalyst has become an attractive research area [2]. Amongst various types of organocatalyst, 1,1'-bi-2-naphthol (BINOL) and its derivatives have been greatly used as organocatalysts for a wide range of asymmetric organic reactions [1,3–8]. Based on literature review, most of the commercially available BINOL derivatives are expensive while many others are not commercially available. Preparation of these BINOL derivatives involved tedious multi-step reactions and purifications [9]. Thus, it would be an advantage for these catalytic compounds to be recyclable. Most organocatalysts are used in homogeneous form, which often makes them difficult to recycle and reused after a reaction. Even when possible, the overall process for recycling of these organocatalysts is rather cumbersome and uneconomical.

There have been some efforts to prepare recyclable heterogeneous BINOL organocatalysts by immobilising BINOL onto different polymeric materials and silica gel [1b,10–14]. However, filtration is required to recover these heterogeneous BINOL organocatalyst. Recently, magnetic iron oxide particle (MIOP) has emerged as a new supporting material for various recoverable catalysts [15,16]. MIOP-grafted catalyst can be easily separated from the reaction mixture by applying an external magnetic field. Thus far, there has been no report on immobilisation of BINOL onto MIOP. In this study, we report a general method for immobilisation of BINOL-derived catalyst onto MIOP and its performances was evaluated using asymmetric aldol reactions. In addition, molecular modelling was carried out to explain the effect of BINOL catalyst in asymmetric aldol reaction. The reusability of the catalyst in this reaction was also assessed.

2. Experimental

2.1. Chemicals

Iron(II) chloride, iron(III) chloride, 2-propanol, methanol, ethanol, toluene, dichloromethane (DCM), chloroform, *N,N*-

* Corresponding author. Fax: +60 379674193.
E-mail address: yeanke@um.edu.my (Y.K. Lee).

dimethylformamide (DMF), tetrahydrofuran (THF), diisopropylethylamine (DIEA), (R)-BINOL, bromine, trifluoroacetic acid, *N*-(3-dimethylaminopropyl)-*N'*-ethylcarbodiimide hydrochloride (EDC.HCl), Hydroxybenzo-triazole (HOBt), potassium hydroxide, sodium bicarbonate (NaHCO₃) and ammonium hydroxide (25%) were obtained from Merck. Tetraethyl orthosilicate (TEOS), (3-amino-propyl) triethoxysilane (APTEOS), 4-dimethylaminopyridine (DMAP) and triethylamine (TEA) were purchased from Sigma–Aldrich. 4-Methoxymethyl phenylboronic acid was purchased from Alfa Aesar. Deionised water was obtained from an ultra pure water system Elga (UK).

2.2. Preparation of aminated Silica coated MIOP (MIOP–SiO₂–NH₂)

MIOP was synthesised using co-precipitation method [17]. Subsequently, silica was coated onto MIOP to prepare MIOP–SiO₂ [18]. Preparation of MIOP–SiO₂–NH₂ from MIOP–SiO₂ was performed as follows: 2 g of MIOP–SiO₂, 5 g of APTEOS, 0.1 cm³ of TEA, and 25 cm³ of toluene were swirled for 10 min under a nitrogen atmosphere. Then, the mixture was refluxed for 24 h under a nitrogen atmosphere. MIOP–SiO₂–NH₂ was collected by an external magnetic field and washed with toluene followed by methanol. The MIOP–SiO₂–NH₂ was then dried under vacuum.

2.3. Immobilisation of BINOL–Acid onto MIOP–SiO₂–NH₂ (BINOL–MIOP)

The BINOL-derived organocatalyst, 6,6'-bis-(4-carboxyphenyl)-1,1'-bis-2-naphthol (BINOL–Acid) was synthesised as reported by Pereira et al. [13] with a slight modification. Spectral data obtained for BINOL–Acid were identical to those reported in literature [13]. To immobilise BINOL–Acid onto MIOP–SiO₂–NH₂, 250 mg of MIOP–SiO₂–NH₂ and 60 mg of BINOL–Acid, together with the amide coupling agent, EDC.HCl, HOBt and DMAP, were premixed and subjected to high vacuum dry for 30 min. 20 cm³ of freshly distilled DCM, 10 cm³ of dry DMF, and 0.06 cm³ DIEA was then added into the mixture and stirred for 3 days. The particle was washed with methanol and dried under vacuum for 1 h.

2.4. Characterisation of the prepared catalyst

Thermal gravimetric analysis (TGA) measurements were performed on a TGA4000 PerkinElmer instrument. Each sample was heated from 50 to 800 °C with the rate of 10 °C/min under air flow (30 cm³/min). Fourier-Transformed Infrared (FTIR) spectra were recorded using a PerkinElmer FTIR spectrophotometer. FTIR spectra of modified particles were collected in transmission mode by pressing the particle sample with potassium bromide powder to form pellets. A resolution of 2 cm⁻¹ and a total of 16 scans were applied for the collection of FTIR spectra. The morphology of the BINOL–MIOP was obtained by scanning electron microscopy (SEM). SEM micrographs were taken in a Hitachi SU8220. Samples were placed on carbon tape and mounted on aluminium sample holders for analysis.

2.5. Heterogeneous catalytic procedure

Ketone and benzaldehyde were premixed with 100 mg of BINOL–MIOP, 0.5 cm³ of THF and 2 cm³ of 1 M NaHCO₃ were then added. The reaction mixture was agitated with vortex for the specified time. After reaction, BINOL–MIOP was separated from reaction mixture with external magnet field and the reaction mixture was then decanted. The reaction mixture was then neutralised with 5% HCl and extracted with chloroform. The extracts were subjected to spectral analysis (NMR) and HPLC analysis. All HPLC

analyses were performed using Shimadzu HPLC system consisted of a LC-20AT pump, a SPD-M20A diode array detector, a SIL-20AHT auto sampler, a CTO-20AC column oven and a CBM-20A communication bus module (Shimadzu, Japan). A Daicel Chiralpak AS-H column (0.46 cm × 15 cm) and Daicel Chiralpak IC column (0.46 cm × 15 cm) with hexane and isopropanol as eluent were used for separation.

2.6. Molecular modelling

2.6.1. Simulation of single-bound and double-bound BINOL–Acid onto MIOP–SiO₂–NH₂

The BINOL–Acid structure was constructed based on the X-ray crystal structure of BINOL obtained from International Union of Crystallography (IUCr) with cif reference OH1012 [19]. Semiempirical method, PM6 was employed to explore the possible conformations in free-form of BINOL–Acid through the torsional angle between the two naphthol ring planes of BINOL–Acid with the step size of 20° for 18 steps and structurally optimised until the completed torsional scan of 360°. The initial structure of BINOL–Acid was optimised using density function theory (DFT) with B3LYP/6-311+G (d,p) basis set using Gaussian 09 [20]. The optimised model of BINOL–Acid was then used to construct the model of BINOL–Acid bound on the silica surface. The structure of BINOL–Acid on APTEOS bonded to silica was modelled according to the quartz structure reported by Levien et al. [21] and optimised with CHARMm force field of Discovery Studio (DS) 2.5. The supercell was built with eight sites of silica functionalised with hydroxyl (–OH) group side chain and end-capped with methyl (–CH₃) group. The initial distance between the amino groups of APTEOS was set at about 4.92 Å. Since BINOL–Acid has two carboxylic acid ends available to react with the amino group (–NH₂) of APTEOS on the silica surface, two possible immobilised models, i.e. single-bound (SG) and double-bound (DB) BINOL–Acid with APTEOS complexes, were modelled. The initial SG model was bound to the middle site of APTEOS coated on silica and optimised with CHARMm force field in DS 2.5 with smart minimisation exiting with gradient tolerance 0.0001 kcal/(mol × Å) satisfied. The DB model with the lowest energy structure was accessed from the possible DB bound BINOL–Acid with APTEOS, where one carboxylic acid is attached to –NH₂ of site 1 and another carboxylic acid is attempted to attach with another –NH₂ site in the range of 2–5.

2.6.2. Simulation of the BINOL–MIOP catalysed aldol reaction

The molecular dynamics simulation (MDs) was done to simulate the aldol reaction catalysed by the SG and DB BINOL–MIOP when both catalysts were in complex with *p*-nitrobenzaldehyde respectively, with harmonic atom restrain and force constant of 0.001 kcal/mol/Å². The *p*-nitrobenzaldehyde was initially added in between of the two central –OHs of BINOL–MIOP and the MDs was done for 1000 ps with the time step of 1 fs with the number of mole (*n*), volume (*V*) and temperature (*T*) ensembles at 300 K. Trajectories of the complex configuration for the final 500 ps were recorded at every 0.5 ps and a total of 1000 structures were analysed in detail.

3. Results and discussion

3.1. Preparation of BINOL–MIOP

The preparation of BINOL–MIOP was begun with the MIOP synthesis using co-precipitation of ferric and ferrous salts in basic solution [17] followed by silica coating using TEOS to produce MIOP–SiO₂. MIOP was then subjected to amine functionalisation to produce MIOP–SiO₂–NH₂. R-BINOL was used to synthesise BINOL–Acid. Subsequently, the BINOL–Acid was immobilised onto

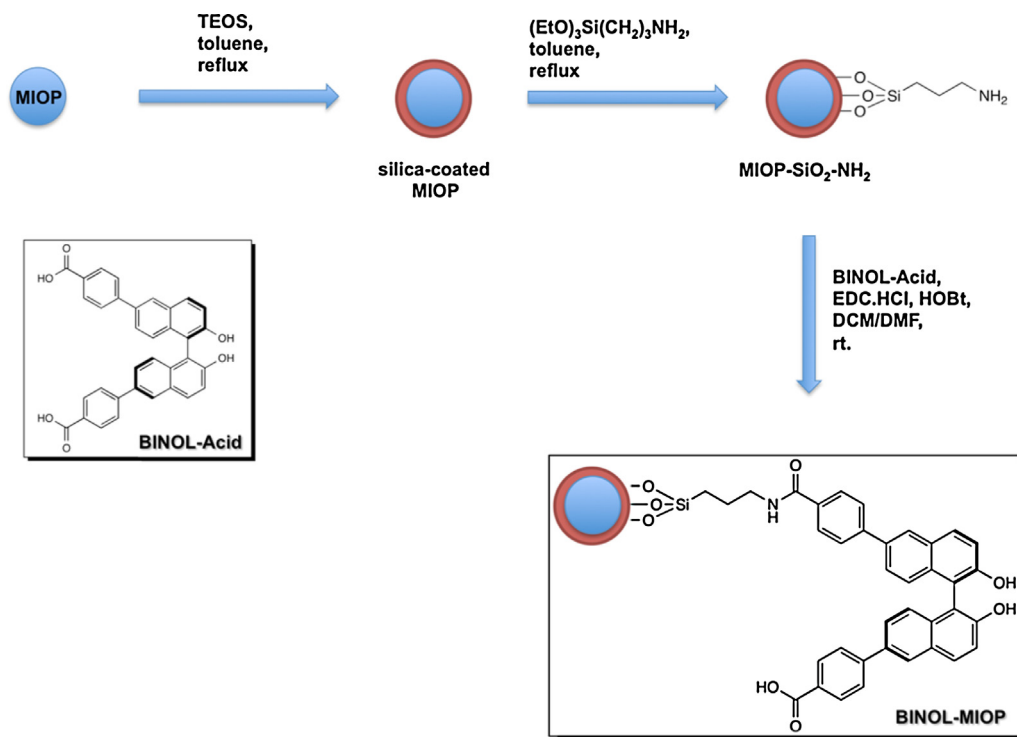


Fig. 1. Steps to produce BINOL-MIOP.

MIOP-SiO₂-NH₂ via standard amide coupling procedure to produce BINOL-MIOP (Fig. 1).

3.2. Characterisation of the MIOPs

3.2.1. FTIR analysis

The FTIR analyses were carried out to verify the presence of BINOL-Acid on MIOP-SiO₂-NH₂ after immobilisation. FTIR spectra of MIOP-SiO₂ showed the main characteristic peaks at 1096 cm⁻¹ (Si-O stretching) and 3415 cm⁻¹ (O-H deformation) (Fig. 2a). For MIOP-SiO₂-NH₂, the appearance of a peak at 1596 cm⁻¹ (NH₂ bending) confirmed the amino functionalisation (Fig. 2b). The emergence of peaks at 1506 (BINOL C=C stretching), 1650 (BINOL

amide C=O stretching) [13], 2857 and 2925 cm⁻¹ (C-H stretching) in BINOL-MIOP suggesting the BINOL-Acid was successfully grafted onto the surface of MIOP-SiO₂-NH₂, where the similar peaks were observed in the spectra of free BINOL-Acid (Fig. 2c and 2d). Based on the co-emergence of amide carbonyl stretching (1650 cm⁻¹) and carboxylic acid stretching (1700 cm⁻¹), the BINOL-Acid was grafted onto MIOP-SiO₂-NH₂ via one end and both ends.

3.2.2. Thermogravimetry Analysis (TGA)

TGA was carried out to estimate the loading of the BINOL-Acid that grafted onto the MIOP-SiO₂-NH₂. Generally, MIOP-SiO₂, MIOP-SiO₂-NH₂, and BINOL-MIOP showed two successive weight losses, where one was found at below 150 °C and another one at above 150 °C. At below 150 °C, the weight loss may be due to the water desorption. Subsequent weight loss at above 150 °C was presumed to correspond to dehydroxylation of the silanol groups, decomposition of aminopropyl silane groups and BINOL-Acid [13] (Fig. 3). MIOP-SiO₂-NH₂ showed additional 7.5% weight loss as compared to MIOP-SiO₂, which was due to the decomposition of aminopropyl silane groups. As reported by Pereira et al. [13], 9.2% weight loss corresponded to 1 mmol NH₂ per gram of commercially available aminopropyl silica gel [13]. Therefore, 7.5% weight loss would correspond to 0.81 mmol NH₂ per gram of MIOP-SiO₂-NH₂. BINOL-MIOP showed additional 11.7% weight loss as compared with MIOP-SiO₂-NH₂. By taking into account the weight loss that is attributed to dehydroxylation of silanol groups, decomposition of aminopropyl groups and BINOL-Acid groups from BINOL-MIOP, the estimated loading of BINOL-Acid was 0.23 mmol per gram.

3.2.3. SEM analysis

SEM images of MIOP-SiO₂-NH₂ and BINOL-MIOP were obtained to visualise the differences on surface morphology before and after BINOL-Acid grafting (Fig. 4). BINOL-MIOP (Fig. 4a) exhibited rougher particle morphology and agglomeration after BINOL-Acid grafting (Fig. 4b). This phenomenon could be explained

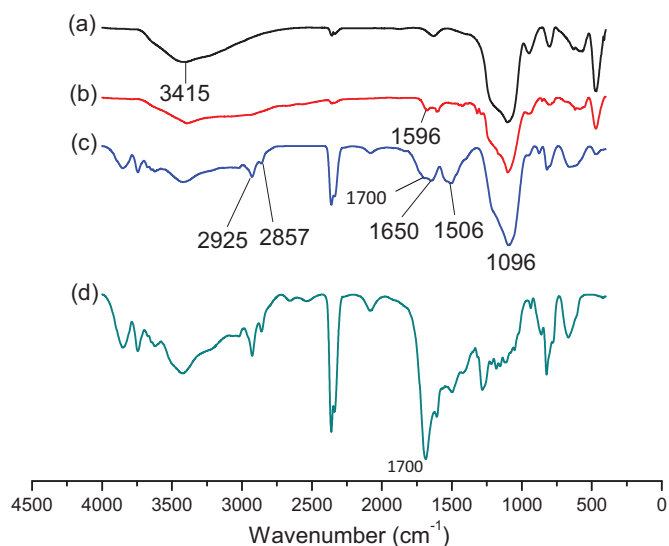


Fig. 2. IR spectrum of (a) MIOP-SiO₂, (b) MIOP-SiO₂-NH₂, (c) BINOL-MIOP, and (d) BINOL-Acid.

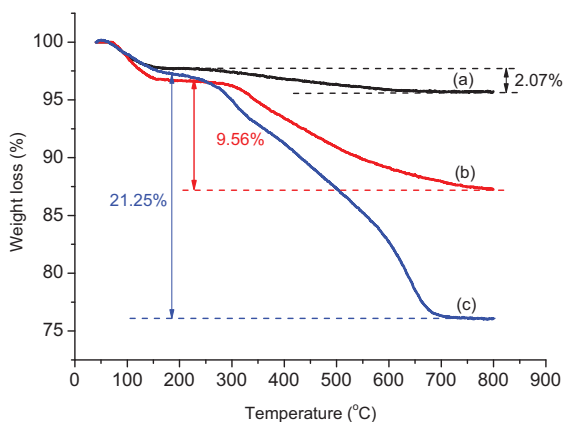


Fig. 3. TGA curves of (a) MIOP-SiO₂, (b) MIOP-SiO₂-NH₂, and (c) BINOL-MIOP.

by the hydrophobic interactions between the aromatic rings of BINOL groups. The estimated average sizes of these particles were ranging from 200 to 250 nm.

3.3. Evaluation of BINOL-MIOP catalysed aldol reaction

BINOL-MIOP was first evaluated in aldol reaction using the optimised conditions [22]. For comparison purpose, the aldol reactions with and without homogeneous BINOL were carried out between *p*-nitrobenzaldehyde and 2-cyclopentenone (entry 1, a and b, Table 1). To our delight, the similar performances were obtained to both catalytic systems. A better *syn* to *anti* selectivity was observed in BINOL-MIOP as compared to homogeneous BINOL. Although homogeneous system showed 50% ee for *anti* adduct, the heterogeneous system still gave an observable ee (i.e., 35%). This validates the participation of BINOL-MIOP in the asymmetric aldol reaction between benzaldehyde and ketone. The absence of sodium bicarbonate resulted no aldol adduct formed (entry 1, c), indicating the importance of sodium bicarbonate as a base in this aldol reaction system, while BINOL-MIOP is only involved in controlling the stereoselectivity.

The versatility of BINOL-MIOP mediated aldol reaction system at room temperature was also evaluated using various benzaldehydes and ketones. In most cases, the corresponding aldol adducts were produced in moderate to good yields. The benzaldehyde bearing an electron-withdrawing group at para-position reacted quickly with 2-cyclopentenone (entry 1, Table 1) or cyclopentanone (entry 4, Table 1) to give the product in almost quantitative yields. Electron-donating group on benzaldehyde took longer time to react

(ca. 72 h) with good yields (entries 3 and 6, Table 1). The bulky naphthaldehyde reacted with ketones to give moderate conversions (entries 2 and 5, Table 1). Reaction between cyclopentanone and benzaldehydes, however, did not display any stereoselectivity (entries 4–6, Table 1). Reaction between 2-cyclopentenone with *p*-nitrobenzaldehyde or 3,5-dimethoxybenzaldehyde, on the other hand, gave rise to an observable enantioselectivity on their *anti* adducts (entries 1 and 3, Table 1). The reactions gave moderate diastereoselectivities, where the *syn*:*anti* ratios were from 70:30 to 79:21.

3.4. Plausible reaction mechanism

Reaction mechanism of aldol reaction in the presence of base is well known and reported elsewhere [23, and the references therein]. Hence, in our reaction system, we postulated the formation of cyclopentenolate from 2-cyclopentenone under mild basic condition of sodium bicarbonate for the initiation of reaction. The generated enolates were nucleophilic enough to undergo nucleophilic addition to the electrophilic benzaldehydes to produce aldol adduct (Fig. 5). This explained the formation of aldol adduct even without the presence of BINOL catalyst (entry 1b, Table 1). The presence of BINOL as a chiral control catalyst is proposed to form a hydrogen bond to the benzaldehyde that caused the biased *syn*-addition versus *anti*-addition. The further ee observed in *anti*-addition is postulated to have a biased access of the 2-cyclopentenolate to the *anti*-site of the benzaldehyde (Fig. 6). To further investigate this proposed mechanism, molecular modelling was carried out.

3.5. Molecular modelling for SG BINOL and DB BINOL model on silica surface

Potential energy of optimised structure of free BINOL-Acid was plotted as a function of the torsional angle between the two naphthol ring planes of BINOL-Acid that was located at about the central of the structure (Fig. 7). Two lowest energy BINOL-Acid structures with torsion of 88.6° and -91.4° were observed. Possible low energy structures with relative energy <3.00 kcal/mol compared to the lowest energy structure at degree torsion angle were found between -131.4° to -61.4° and 68.6° to 128.6°, indicating the possible torsional angle that free BINOL-Acid may adopt. The SG and DB bound BINOL-Acid with APTEOS was simulated using the more accurate DFT-optimised BINOL-Acid structure based on the X-ray crystal structure of BINOL that was found to have a torsional angle of 81.0°. While the SG bound BINOL-Acid was assumed to have the similar torsional angle with the free BINOL-Acid, the exploration

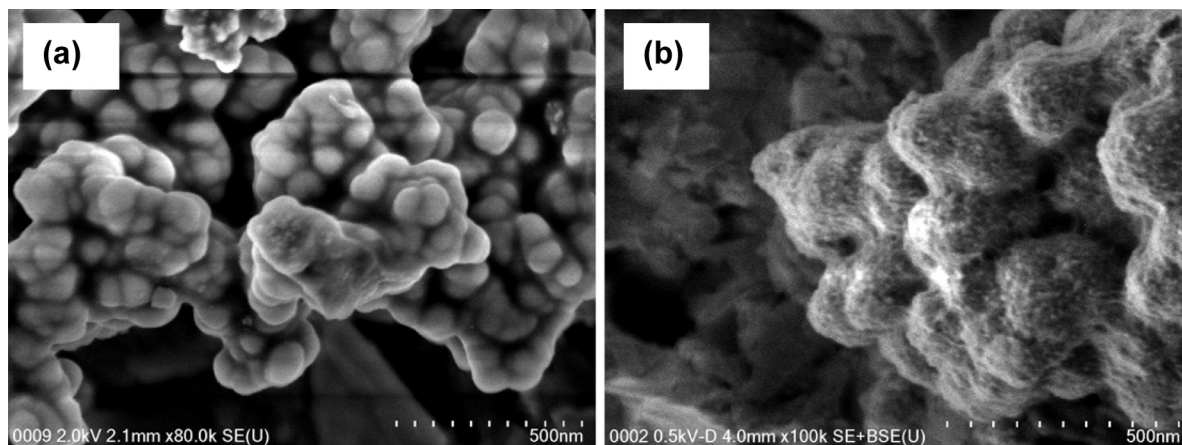
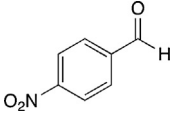
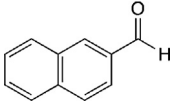
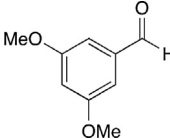
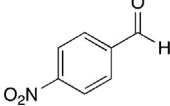
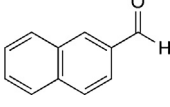
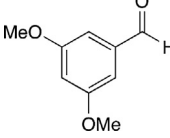


Fig. 4. SEM image of (a) MIOP-SiO₂-NH₂ and (b) BINOL-MIOP.

Table 1
Aldol reaction between various aldehydes and ketones.

Entry	Aldehyde	Ketone	Time, (h)	% Conversions	Syn:anti	% ee (Syn, anti)
1			14 (16 ^a , 21 ^{b,c})	98 (96 ^a , >99 ^b , 0 ^c)	79:21 (76:24) ^a , (70:30) ^b	0.6, 35.0 (0, 50) ^a
2			72	45	77:23	0.3, 3.3
3			72	93	72:28	0, 35.0
4			14	99	73:27	2.7, 1.1
5			72	57	70:30	0.2, 1.2
6			72	94	71:29	2.2, 0.2

^a Results obtained from homogeneous 20% BINOL-catalysed reaction.

^b Results obtained from homogeneous reaction without BINOL.

^c Results obtained from BINOL–MIOP catalysed reaction without sodium bicarbonate.

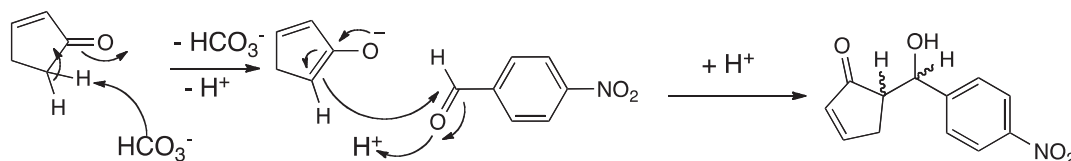


Fig. 5. Postulated reaction mechanism between *p*-nitrobenzaldehyde and 2-cyclopentene-1-one.

of DB bound BINOL–Acid with APTEOS suggested three possible DB models with negative potential energy that were found with the torsional angle of 53.4°, 109.4°, and 117.5° (Fig. 8). The Model 3 with torsional angle of 117.5° was found to be the lowest energy structure of -16.83 kcal/mol, indicating the possible angle distortion occurred when BINOL–Acid was bound in the DB manner, as compared to the free BINOL–Acid or SG bound BINOL–Acids (Fig. 8). Thus, in order to address the effect of BINOL angle distortion to the stereocontrol of BINOL–MIOP catalysed aldol reaction, subsequent simulation was performed using the configuration of Model 3 as DB bound model to further investigate the BINOL–aldehyde complexation via MDs.

3.6. Simulation of the BINOL–MIOP catalysed aldol reaction

From the potential energy plot (data not shown) of the 1000 ps MDs, the equilibrium structure of BINOL–aldehyde complexes

of SG and DB models were achieved after 300 ps run. 1000 dynamics structures from the final 500 ps trajectories were analysed (Fig. 9). The average interaction energies (IE) of the SG complex and DB complex were found to be -34.22 ± 3.02 and -16.48 ± 1.95 kcal/mol with the respective average torsional angle of $90.52^\circ \pm 9.89^\circ$ and $115.19^\circ \pm 4.54^\circ$. DB model has a lower fluctuation in terms of torsional angle (Fig. 9, B) that may attribute to the higher IE (Fig. 9, D) due to the constraint of its structure when both carboxylic acid ends were bound to silica surface. SG model complex was found to have lower interaction energy (Fig. 9, C) as compared to DB model complex (Fig. 9, D), thereby suggesting a more favourable complex formation of SG model. This result indicated that the involvement of SG bound BINOL–Acid and free BINOL–Acids in aldol reactions were more favourable, thereby contributing a higher ee of the *anti* adducts (entry 1, Table 1). In the case of DB bound BINOL–Acid, the formation of BINOL–aldehyde complex was relatively less favourable as compared to SG, which

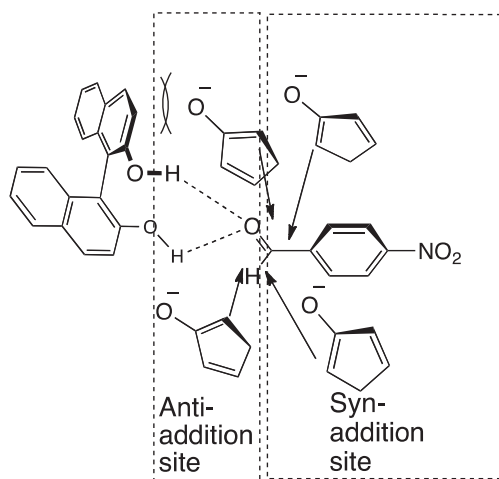


Fig. 6. Plausible BINOL-mediated aldol reaction of the *syn* and *anti* accessibilities of the cyclopentenolate towards the complexed *p*-nitrobenzaldehyde.

may suggest a weaker BINOL-mediated asymmetric aldol reaction. In addition, a weaker BINOL bound benzaldehyde may subsequently increase the probability of the aldol reaction to occur in solution directly without going through the BINOL–aldehyde complexation, which may explained the lower ee of *anti* adduct

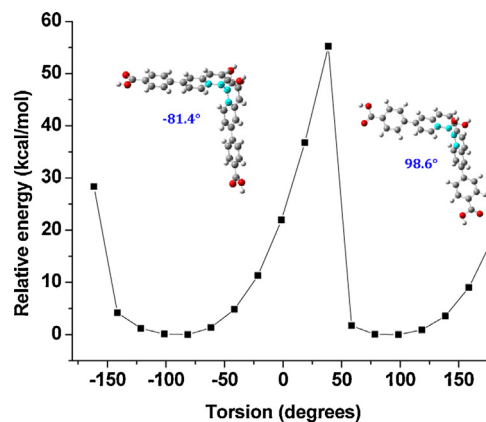


Fig. 7. Relative potential energy with torsional angle scan (in blue) for free BINOL–Acid model. (For interpretation of the references to colour in this figure legend, the reader is referred to the web version of this article.)

observed in the heterogeneous BINOL–MIOP mediated aldol reaction between *p*-nitrobenzaldehyde and 2-cyclopentenone (entry 1, Table 1).

3.7. Catalyst reusability test

Reusability is usually a critical feature for a catalyst. Thus, we attempted to study the reusability of the BINOL–MIOP catalyst by recycling it up to 10 consecutive runs of aldol reaction

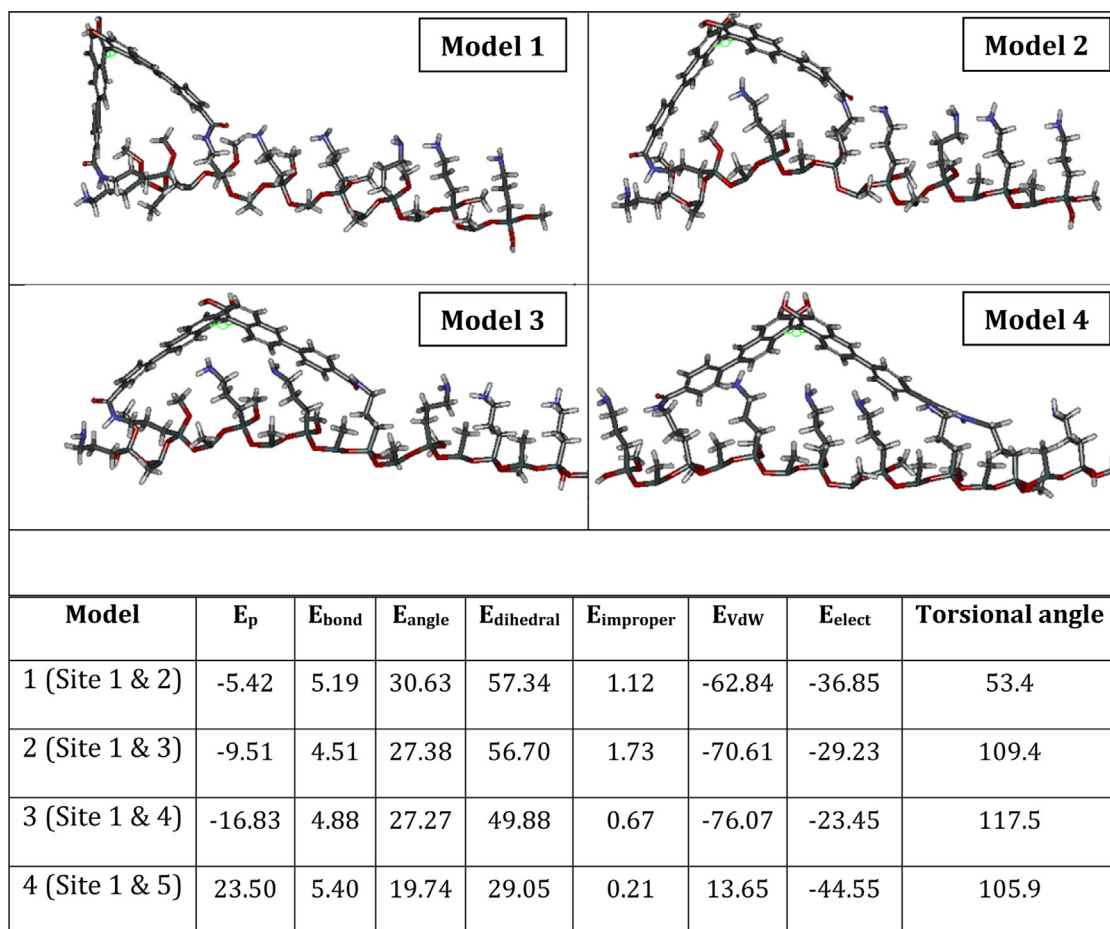


Fig. 8. The minimised structures of different DB models with CHARMm force field were depicted. The energy contribution to potential energy (E_p) according to bonding (E_{bond}), angle (E_{angle}), dihedral (E_{dihedral}), improper (E_{improper}), Van der Waals (E_{vdw}) and electrostatic (E_{elect}) interactions in kcal/mol were listed.

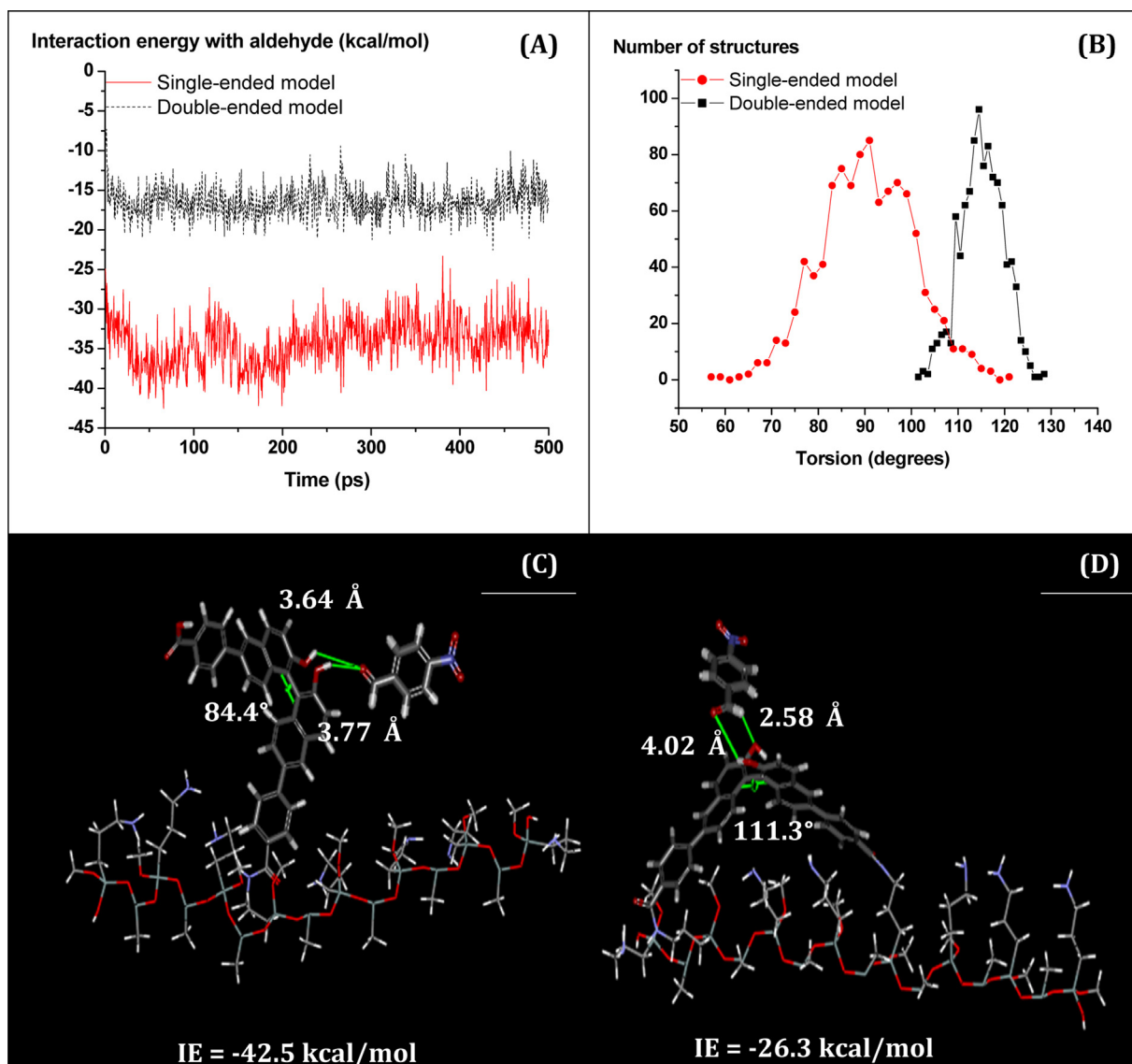


Fig. 9. MDs analysis of the simulated 1000 BINOL-aldehyde complex structures obtained from the final 500 ps. (A) The interaction energy between BINOL-Acid and *p*-nitrobenzaldehyde, (B) distribution of torsional angle, the lowest IE structure of (C) SG model and (D) DB model, were shown.

Table 2
BINOL-MIOP reusability experiment for aldol reaction.

Attempt	% conversions	Syn:anti	% ee (<i>Syn, anti</i>)
1	98	79:21	0.6, 35.0
2	95	81:19	1.0, 36.0
3	95	78:22	5.0, 34.0
4	96	76:24	6.0, 38.0
5	95	84:16	0.8, 40.0
10	98	81:19	0.4, 38.0

between *p*-nitrobenzaldehyde and 2-cyclopentenone. After each run, the catalyst was recovered by applying an external magnet to decant the reaction mixture and rinsed several times with THF and water, followed by vacuum dry prior to the next reaction run. The results indicated no significant loss in stereoselectivity and the product yield was observed after repeated runs of recovered BINOL-MIOP. The obtained yields of the reusability experiments are within the experimental deviations (Table 2).

4. Conclusions

We successfully developed a method to immobilise BINOL onto MIOP. The magnetically recoverable BINOL-MIOP was capable and versatile to mediate asymmetric aldol reactions with moderate-to-good yields and fair diastereoselectivity as well as enantioselectivity. In addition, the free-BINOL gave slightly higher enantioselectivity of *anti*-adduct than BINOL-MIOP. The results obtained from molecular modelling suggested that this reduced enantioselectivity is caused by the torsional angle distortion of BINOL-Acid when it was immobilised onto MIOP in DB manner. In contrast to the free-BINOL or SG BINOL, the distorted BINOL was found to be less favourable to form complex with aldehyde. Thus, BINOL-MIOP has a poorer *anti*-enantioselectivity than the free-BINOL, which may attribute to the higher probability of aldol reaction to occur without going through BINOL-aldehyde complexation. In addition, BINOL-MIOP could be recycled and reused for at least 10 times without significant loss in aldol adduct conversions, particularly in their stereoselectivity. Further work utilising this powerful technique are underway to immobilise more robust,

versatile, stereoselective and recyclable BINOL-related organocatalysts for asymmetric organic reactions.

Acknowledgements

The author would like to acknowledge the financial support from Ministry of Education Malaysia (ERGS ER005-2013A) and University of Malaya Research Officer Grant Scheme (ROGS BR008-2014).

References

- [1] (a) M. Rueping, E. Sugiono, A. Steck, T. Theissmann, *Adv. Synth. Catal.* 352 (2010) 281–287; (b) D.S. Kundu, J. Schmidt, C. Bleschke, A. Thomas, S. Blechert, *Angew. Chem., Int. Ed.* 5 (1) (2012) 5456–5459.
- [2] W.H. Zhong, S. Liu, J. Yang, X.B. Meng, Z.J. Li, *Org. Lett.* 14 (2012) 3336–3339.
- [3] A. Zamfir, S. Schenker, M. Freund, S.B. Tsogoeva, *Org. Biomol. Chem.* 8 (2010) 5262–5276.
- [4] A. Zamfir, S.B. Tsogoeva, *Org. Lett.* 12 (2010) 188–191.
- [5] G. Wang, B. Wang, S. Qi, J. Zhao, Y. Zhou, J. Qu, *Org. Lett.* 14 (2012) 2734–2737.
- [6] M. Hatano, K. Moriyama, T. Maki, K. Ishihara, *Angew. Chem. Int. Ed.* 49 (2010) 3823–3826.
- [7] A.K. Mutyala, N.T. Patil, *Org. Chem. Front.* 1 (2014) 582–586.
- [8] V. Eschenbrenner-Lux, P. Kuchler, S. Ziegler, K. Kumar, H. Waldmann, *Angew. Chem, Int. Ed.* 53 (2014) 2134–2137.
- [9] W. Hu, J. Zhou, X. Xu, W. Liu, L. Gong, *Org. Synth.* 88 (2012) 406–417.
- [10] H. Sellner, C. Faber, P.B. Rheiner, D. Seebach, *Chem. Eur. J.* 6 (2000) 3692–3705.
- [11] I.P. Beletskaya, L.S. Patrikeeva, F. Lamaty, *Russ. Chem. Bull.* 60 (2011) 2370–2374.
- [12] S. Takizawa, M.L. Patil, F. Yonezawa, K. Marubayashi, H. Tanaka, T. Kawai, H. Sasai, *Tetrahedron Lett.* 46 (2005) 1193–1197.
- [13] M.M. Pereira, A.C.B. Neves, M.J.F. Calvete, L.D. Dias, A. Fernandes, *Catal. Today* 218 (2013) 99–106.
- [14] V. Morales, J.A. Villajos, R.A. Garcia, *J. Mater. Sci.* 48 (2013) 5990–6000.
- [15] T. Arai, T. Sato, H. Kanoh, K. Kaneko, K. Oguma, A. Yanagisawa, *Chem. Eur. J.* 14 (2008) 882–885.
- [16] M.B. Gawande, P.S. Branco, R.S. Varma, *Chem. Soc. Rev.* 42 (2013) 3371–3393.
- [17] O. Karaagac, H. Kockar, S. Beyaz, T. Tanrisever, *IEEE Trans. Magn.* 46 (2010) 3978–3983.
- [18] X. Kong, R.X. Gao, X.W. He, L.X. Chen, Y.K. Zhang, *J. Chromatogr. A* 1245 (2012) 8–16.
- [19] K. Mori, Y. Masuda, S. Kashino, *Acta Cryst. C* 49 (1993) 1224–1227.
- [20] M.J. Frisch, G.W. Trucks, H.B. Schlegel, G.E. Scuseria, M.A. Robb, J.R. Cheeseman, G. Scalmani, V. Barone, B. Mennucci, G.A. Petersson, H. Nakatsuji, M. Caricato, X. Li, H.P. Hratchian, A.F. Izmaylov, J. Bloino, G. Zheng, J.L. Sonnenberg, M. Hada, M. Ehara, K. Toyota, R. Fukuda, J. Hasegawa, M. Ishida, T. Nakajima, Y. Honda, O. Kitao, H. Nakai, T. Vreven, J.A. Montgomery Jr., J.E. Peralta, F. Ogliaro, M. Bearpark, J.J. Heyd, E. Brothers, K.N. Kudin, V.N. Staroverov, R. Kobayashi, J. Normand, K. Raghavachari, A. Rendell, J.C. Burant, S.S. Iyengar, J. Tomasi, M. Cossi, N. Rega, J.M. Millam, M. Klene, J.E. Knox, J.B. Cross, V. Bakken, C. Adamo, J. Jaramillo, R. Gomperts, R.E. Stratmann, O. Yazyev, A.J. Austin, R. Cammi, C. Pomelli, J.W. Ochterski, R.L. Martin, K. Morokuma, V.G. Zakrzewski, G.A. Voth, P. Salvador, J.J. Dannenberg, S. Dapprich, A.D. Daniels, Ö. Farkas, J.B. Foresman, J.V. Ortiz, J. Cioslowski, D.J. Fox, *Gaussian 09, Revision A.1*, 21, Gaussian, Inc., Wallingford CT, 2009, pp. 111.
- [21] L. Levien, C.T. Prewitt, D. Weidner, *J. Am. Mineral.* 65 (1980) 920–930.
- [22] K. Nakayama, K. Maruoka, *J. Am. Chem. Soc.* 130 (2008) 17666–17667.
- [23] B. Trost, C. Brindle, *Chem. Soc. Rev.* 39 (2010) 1600–1632.